ANL/NDM--116

DE90 014222

ANL/NDM–116

# NEUTRON SCATTERING FROM ELEMENTAL INDIUM, THE OPTICAL MODEL, AND THE BOUND–STATE POTENTIAL*

by

S. Chiba†, P. T. Guenther, R. D. Lawson, and A. B. Smith

June 1990

Keywords

Measured $\sigma_{el}$ of elemental indium for neutrons of 4.5–10 MeV. Optical–model interpretation. Extrapolation to bound particle and hole states.

Engineering Physics Division
ARGONNE NATIONAL LABORATORY
9700 South Cass Avenue
Argonne, Illinois 60439
U.S.A.

*This work supported by the U. S. Department of Energy under Contract No. W–31–109–Eng–38.
†Visiting scientist from Japan Atomic Energy Research Institute, Tokai Establishment.

## NUCLEAR DATA AND MEASUREMENTS SERIES

The Nuclear Data and Measurements Series presents results of studies in the field of microscopic nuclear data. The primary objective is the dissemination of information in the comprehensive form required for nuclear technology applications. This Series is devoted to: a) measured microscopic nuclear parameters, b) experimental techniques and facilities employed in measurements, c) the analysis, correlation and interpretation of nuclear data, and d) the evaluation of nuclear data. Contributions to this Series are reviewed to assure technical competence and, unless otherwise stated, the contents can be formally referenced. This Series does not supplant formal journal publication, but it does provide the more extensive information required for technological applications (e.g., tabulated numerical data) in a timely manner.

## TABLE OF CONTENTS

## INFORMATION ABOUT OTHER ISSUES OF THE ANL/NDM SERIES

A list of titles and authors for all the previous issues appears in each report of the series. The list for reports ANL/NDM–1 through ANL/NDM–75 appears in ANL/NDM–76, and ANL/NDM–91 contains the list for reports ANL/NDM–76 through ANL/NDM–90. Below is the list for ANL/NDM–91 up to the current report. Requests for a complete list of titles or for copies of previous reports should be directed to:

Section Secretary
Applied Nuclear Physics Section
Engineering Physics Division
Building 316
Argonne National Laboratory
9700 South Cass Avenue
Argonne, Illinois 60439
U.S.A.

**ANL/NDM–91** A.B. Smith, P.T. Guenther and R.D. Lawson, *On the Energy Dependence of the Optical Model of Neutron Scattering from Niobium*, May 1985.

**ANL/NDM–92** Donald L. Smith, *Nuclear Data Uncertainties (Vol.–I): Basic Concepts of Probability*, December 1988.

**ANL/NDM–93** D.L. Smith, J.W. Meadows and M.M. Bretscher, *Integral Cross–section Measurements for $^{7}Li(n,n't)^{4}He$, $^{27}Al(n,p)^{27}Mg$, $^{27}Al(n,\alpha)^{24}Na$, $^{58}Ni(n,p)^{58}Co$, and $^{60}Ni(n,p)^{60}Co$ Relative to $^{238}U$ Neutron Fission in the Thick–target $^{9}Be(d,n)^{10}B$ Spectrum at $E_d = 7$ MeV*, October 1985.

**ANL/NDM–94** A.B. Smith, D.L. Smith, P. Rousset, R.D. Lawson and R.J. Howerton, *Evaluated Neutronic Data File for Yttrium*, January 1986.

**ANL/NDM–95** Donald L. Smith and James W. Meadows, *A Facility for High–intensity Neutron Irradiations Using Thick–target Sources at the Argonne Fast–neutron Generator*, May 1986.

**ANL/NDM–96** M. Sugimoto, A.B. Smith and P.T. Guenther, *Ratio of the Prompt–fission–neutron Spectrum of Plutonium–239 to that of Uranium–235*, September 1986.

**ANL/NDM–97** J.W. Meadows, *The Fission Cross Sections of $^{230}Th$, $^{232}Th$, $^{233}U$, $^{234}U$, $^{236}U$, $^{238}U$, $^{237}Np$, $^{239}Pu$, and $^{242}Pu$ Relative $^{235}U$ at 14.74 MeV Neutron Energy*, December 1986.

**ANL/NDM–98** J.W. Meadows, *The Fission Cross Section Ratios and Error Analysis for Ten Thorium, Uranium, Neptunium and Plutonium Isotopes at 14.74–MeV Neutron Energy*, March 1987.

**ANL/NDM–99** Donald L. Smith, *Some Comments on the Effects of Long–range Correlations in Covariance Matrices for Nuclear Data*, March 1987.

**ANL/NDM–100** A.B. Smith, P.T. Guenther and R.D. Lawson, *The Energy Dependence of the Optical–model Potential for Fast–neutron Scattering from Bismuth*, May 1987.

**ANL/NDM–101** A.B. Smith, P.T. Guenther, J.F. Whalen and R.D. Lawson, *Cobalt: Fast Neutrons and Physical Models*, July 1987.

**ANL/NDM–102** D. L Smith, *Investigation of the Influence of the Neutron Spectrum in Determinations of Integral Neutron Cross–Section Ratios*, November 1987.

**ANL/NDM–103** A.B. Smith, P.T. Guenther and B. Micklich, *Spectrum of Neutrons Emitted From a Thick Beryllium Target Bombarded With 7 MeV Deuterons*, January 1988.

**ANL/NDM–104** L.P. Geraldo and D.L. Smith, *Some Thoughts on Positive Definiteness in the Consideration of Nuclear Data Covariance Matrices*, January 1988.

**ANL/NDM–105** A.B. Smith, D.L. Smith, P.T. Guenther, J.W. Meadows, R.D. Lawson, R.J. Howerton, and T. Djemil, *Neutronic Evaluated Nuclear–Data File for Vanadium*, May 1988.

**ANL/NDM–106** A.B. Smith, P.T. Guenther, and R.D. Lawson, *Fast–Neutron Elastic Scattering from Elemental Vanadium*, March 1988.

**ANL/NDM–107** P. Guenther, R. Lawson, J. Meadows, M. Sugimoto, A. Smith, D. Smith, and R. Howerton, *An Evaluated Neutronic Data File for Elemental Cobalt*, August 1988.

**ANL/NDM–108** M. Sugimoto, P.T. Guenther, J.E. Lynn, A.B. Smith, and J.F. Whalen, *Some Comments on the Interaction of Fast–Neutrons with Beryllium*, November 1988.

**ANL/NDM–109** P.T. Guenther, R.D. Lawson, J.W. Meadows, A.B. Smith, D.L. Smith, and M. Sugimoto, *An Evaluated Neutronic Data File for Bismuth*, November 1989.

**ANL/NDM–110** D.L. Smith and L.P. Geraldo, *A Vector Model for Error Propagation*, March 1989.

**ANL/NDM–111** J.E. Lynn, *Fifty Years of Nuclear Fission*, June 1989.

**ANL/NDM–112** S. Chiba, P.T. Guenther, and A.B. Smith, *Some Remarks on the Neutron Elastic– and Inelastic–Scattering Cross Sections of Palladium*, May 1989.

**ANL/NDM–113** J.E. Lynn, *Resonance Effects in Neutron Scattering Lengths*, June 1989.

**ANL/NDM–114** A.B. Smith, R.D. Lawson, and P.T. Guenther, *Ambiguities in the Elastic Scattering of 8 MeV Neutrons from Adjacent Nuclei*, October 1989.

**ANL/NDM–115** A.B. Smith, S. Chiba, D.L. Smith, J.W. Meadows, P.T. Guenther, R.D. Lawson, and R.J. Howerton, *Evaluated Neutronic File for Indium*, January 1990.

# NEUTRON SCATTERING FROM ELEMENTAL INDIUM, THE OPTICAL MODEL, AND THE BOUND–STATE POTENTIAL

S. Chiba, P. T. Guenther, R. D. Lawson
and A. B. Smith

## ABSTRACT

Neutron differential elastic–scattering cross sections of elemental indium are measured from 4.5 to 10 MeV at incident–energy intervals of ≈ 500 keV. Seventy or more differential values are obtained at each incident energy, distributed between ≈ 18° and 160°. These experimental results are combined with lower–energy values previously obtained at this laboratory, and with 11 and 14 MeV results in the literature, to form a comprehensive elastic–scattering database extending from ≈ 1.5 to 14 MeV. These data are interpreted in terms of a conventional spherical optical model. The resulting potential is extrapolated to the bound–state regime. It is shown that in the middle of the 50–82 neutron shell, the potential derived from the scattering results adequately describes the binding energies of particle states, but does not do well for hole states. The latter shortcoming is attributed to the hole states having occupational probabilities sufficiently different from unity, so that the exclusion principle becomes a factor, and to the rearrangement of the neutron core.

# I. INTRODUCTION

For half a century indium has been widely used in a variety of nuclear applications. Some of the indium reactions are employed for dosimetry purposes, the two isotopes are fission products, and recently indium has been considered in superconductivity applications. Despite these uses, relatively little is known of the interaction of fast neutrons with indium, and no general–purpose evaluated nuclear–data file for indium exists in the national ENDF/B–V system. Much of the prior knowledge of the interaction of fast neutrons with indium comes from previous work at this laboratory.[1,2] Those studies were at incident–neutron energies of less than 4 MeV. The present work was initiated to extend this previous work up to 10 MeV, and to provide sound nuclear models for extrapolation to other reactions and energies, as necessary for producing the comprehensive evaluated neutronic data file for indium described in Ref. 3.

Over the past few years, this group has made extensive measurements, for a number of nuclei,[4-8] of the neutron differential scattering and total cross sections in the 4 to 10 MeV incident–neutron energy range. These results were combined with those available from earlier measurements at this laboratory, and from the literature, to provide a broad neutron database. These experimental data were interpreted in terms of the spherical optical model (SOM) with resulting parameters that provided the best fit to the available data. These SOM's not only provided a vehicle for the interpretation and interpolation of the new experimental information, but are a mechanism for predicting unmeasured (or unmeasurable) physical properties over the 0 to 20 MeV incident–neutron energy range. Considerations include the unification of potentials applicable to bound and unbound energy regimes in the context of the fundamental dispersion relationship.[9] Here, we extend these studies to the scattering of neutrons from an elemental indium target, and to the associated bound–state properties.

In the present work the observed elastic–scattering cross sections of indium were measured from ≈ 4.5 to 10 MeV in detail, using methods described in Sec. II. The results of these measurements are given and compared with previously reported values in Sec. III. The measured values were interpreted using an SOM potential[10] in which the real interaction was assumed to have a Woods–Saxon shape, the imaginary interaction a derivative Woods–Saxon form, and the spin–orbit potential was the Thomas term. In Sec. IV the deduction of the SOM parameters from the database is described, and the resulting parameters presented. Section V describes the extrapolation of the potential derived from the scattering data to the bound–state regime. The results are discussed, and some conclusions presented, in Sec. VI.

# II. EXPERIMENTAL METHODS

All of the present measurements were made using the fast–neutron time–of–flight technique with the Argonne ten–angle time–of–flight apparatus.[11] The scattered–neutron flight paths were ≈ 5 m. Since the method, the apparatus, and the data acquisition and reduction have been described in detail elsewhere,[11,12,13] only an outline is given here.

The neutron source was the D(d,n)$^3$He reaction, with the deuterium target gas contained in a cell 3 cm long.[14] The gas pressure within the cell was adjusted to give

incident–neutron energy spreads at the sample, including effects due to kinematics, of 100 to 200 keV. The mean energy of the incident neutrons was determined to within 25–50 keV by control of the incident deuteron beam. The neutron source was pulsed at a repetition rate of 2 MHz, with a burst duration of ≈ 1 ns. The scattering sample was a solid cylinder of elemental indium, 2 cm long and 2 cm in diameter. Ten hydrogenous scintillation detectors were used. The relative scattering angles were determined to $< 0.1^{o}$, and the absolute angular scale was calibrated to $\pm 0.1^{o}$ by observing neutrons scattered from the sample both left and right of the apparent geometric center line, at angles where the elastic–scattering cross section is rapidly changing. Although the angular uncertainties were small, they can be a source of significant error in regions where the cross section is changing rapidly with angle. The relative detector energy–dependent sensitivities were determined using the $^{252}$Cf fission–neutron spectrum, as described in Ref. 15. These relative sensitivities were then normalized to the well–known H(n,n) scattering standard[16] by observing neutrons scattered from polyethylene ($CH_2$) samples. The measured cross sections were corrected for multiple–event, incident–beam–attenuation and angular-resolution perturbations using Monte–Carlo techniques.[17] These calculations were carried through three iterations so as to provide an accuracy of 1–2 % at most angles. However, at the very minima of the distributions (in the range $35^{o}$–$45^{o}$, a very deep and narrow minimum occurs at some energies) the uncertainties in the correction factors may be 30% or more. The detector calibrations were reproducible to ≤ 3% up to ≈ 8.5 MeV. Since the intensity of the $^{252}$Cf fission spectrum falls rapidly as the emitted–neutron energy increases above ≈ 3 MeV, this reproducibility decreased to ≤ 5% at higher incident energies. Counting statistics varied a great deal depending on the magnitude of the cross section. At forward angles where the intensities are high, the statistical uncertainties are < 1%, whereas at the very minima of the higher–energy distributions, where the counting rate is approximately three orders–of–magnitude smaller, the statistical uncertainties increased to 10% or more. The various uncertainty estimates were combined in quadrature to obtain the total uncertainty. Generally, the results of measurements made at different times, with different calibrations and detectors, were consistent to within the respective uncertainties.

## III. EXPERIMENTAL RESULTS

The differential neutron elastic–scattering cross sections of elemental indium (95.7% $^{115}$In, 4.3% $^{113}$In) were measured at ≈ 0.5 MeV incident–neutron–energy intervals from 4.5 to 10 MeV. Seventy or more differential values, distributed between ≈ $18^{o}$ and $160^{o}$, were obtained at each incident energy. For each distribution the measurements were made at several different times, using independent calibrations, with good reproducibility of the results. At all scattering angles and incident energies, the scattered–neutron experimental resolution was not sufficient to resolve neutrons due to the inelastic excitation of the 336.3 keV ($1/2^{-}$) metastable level[2] in $^{115}$In (and the analogous level in $^{113}$In). Therefore, the experimental resolution was intentionally kept to ≈ 500 keV, and thus inelastic scattering involving the first $1/2^{-}$ levels was included with the elastic contribution in all of the experimental observations. This inelastic–neutron component is not generally a concern in the present considerations since, even at 3 MeV, the cross section for the excitation of the 336.3 keV level in $^{115}$In is only ≈ 10 mb, and is falling with energy.[3] Consequently, its contribution to the present measurements is probably less than an mb/sr, which is smaller than the experimental uncertainty associated with the observations. This inelastic–scattering component (i.e., the neutron excitation of the $1/2^{-}$ state) should not be confused with the feeding of the $1/2^{-}$ state by the de–excitation of higher–lying levels,

which leads to much larger cross sections at several MeV.[18] Thus, in the present work, the observed cross sections are considered to be entirely due to elastic–scattering.

The differential elastic–scattering cross sections resulting from the present measurements are shown in Fig. III–1. These results reasonably extrapolate to the lower-energy values previously reported from this laboratory,[2] and, except at large scattering angles, to the 11.1 MeV results of Ferrer et al.[19] There are very few directly comparable previously reported elastic–scattering results. However, Holmqvist and Wiedling[20] have measured elastic–scattering cross sections at 4.56, 7.05, and 8.05 MeV. Their results are qualitatively consistent with those of the present work, as illustrated in Fig. III–2.

## IV. MODEL INTERPRETATION

### A. The Experimental Database.

The database considered in the model interpretation consisted of: (i) the s– and p–wave strength functions,[21] (ii) the neutron total cross section from a few keV to 20 MeV,[3] (iii) the elastic scattering of Ref. 2 from 1.5–3.8 MeV, (iv) the present elastic scattering work extending from 4.5 to 10 MeV, (v) the 11.1 MeV elastic scattering of Ref. 19, and (vi) the 14.6 MeV elastic scattering of Ref. 22. The lower–energy data of Ref. 2 were averaged over 200 keV incident–energy increments in order to smooth any fluctuations, and to reduce the number of data points to manageable proportions for the fitting procedures. The total cross sections are shown in Fig. IV–1, and the composite elastic-scattering data used in the fitting are given in Fig. IV–2.

### B. The Phenomenological Spherical Optical Model (SOM)

Since elemental indium is 95.7% $^{115}$In, it was assumed, for simplicity, that the target was monoisotopic $^{115}$In. With this proviso, the data were analyzed using a conventional SOM having a real potential of the Woods–Saxon form, a Woods–Saxon–derivative imaginary interaction, and a spin–orbit term of the Thomas form.[10] A preliminary study indicated that predictions for the data being considered were not particularly sensitive to the spin–orbit parameters. Values of these parameters, similar to those used in fitting the 1.5–3.8 MeV data,[2] and which give a reasonable description of the unpublished 4 MeV polarization results of Gorlov et al.,[23] are

$$\begin{aligned} V_{so} &= 5.5 \text{ MeV} \\ r_{so} &= 1.0 \text{ fm} \\ a_{so} &= 0.65 \text{ fm}, \end{aligned} \qquad \text{(IV–1)}$$

where $V_{so}$, $r_{so}$ and $a_{so}$ are, respectively, the strength, radius and diffuseness of the Thomas term. (Throughout this paper, the nuclear radii, $R_i$, of the various constituents of the SOM potential are given by $R_i = r_i \cdot A^{1/3}$.)

With the spin–orbit potential held fixed to the values of Eq. IV–1, the remaining SOM parameters were determined by fitting the elastic–scattering database shown in

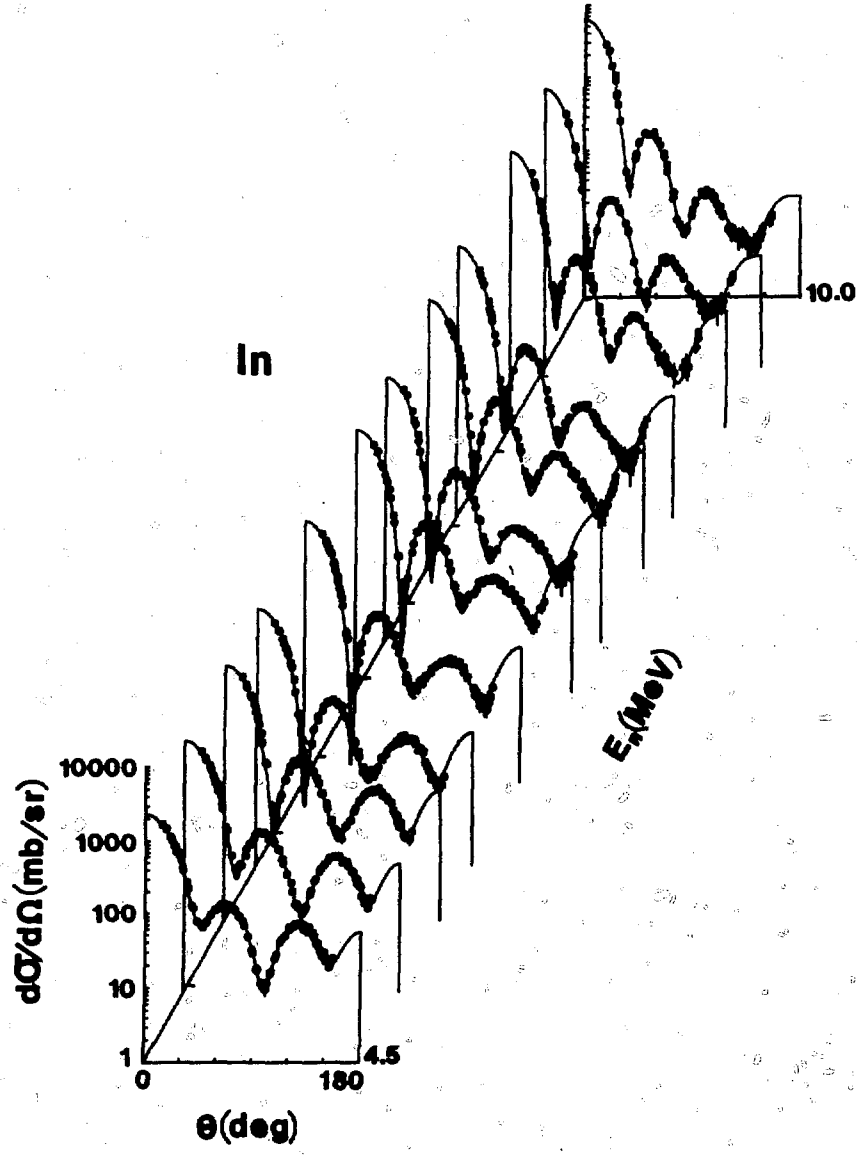


Fig. III–1. Differential neutron elastic–scattering cross sections of indium measured in the present work. The experimental results, with their uncertainties, are indicated by "O" symbols. Curves indicate the results of model calculations, as described in Sec. IV of the text. The data are given in the laboratory coordinate system.

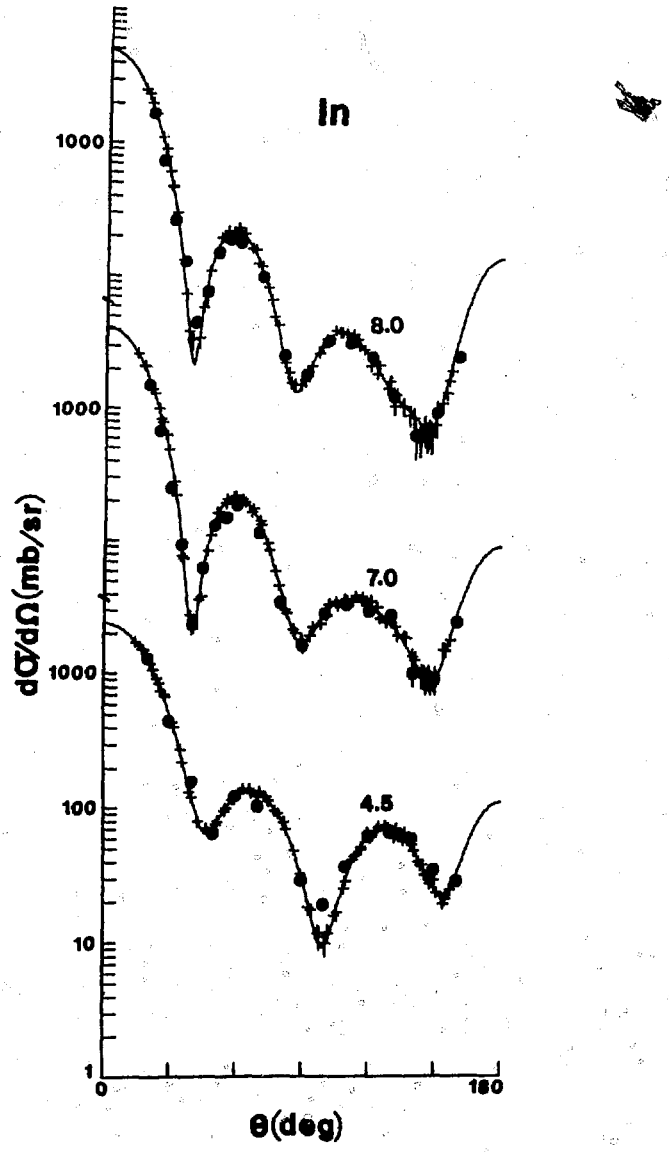


Fig. III–2. Comparison of the present differential elastic–scattering cross sections (+) with the results reported in Ref. 20 (•). The curves are "eyeguides" obtained by Legendre–polynomial fitting the present experimental values. Approximate energies are numerically given in MeV. The data are in the laboratory coordinate system.

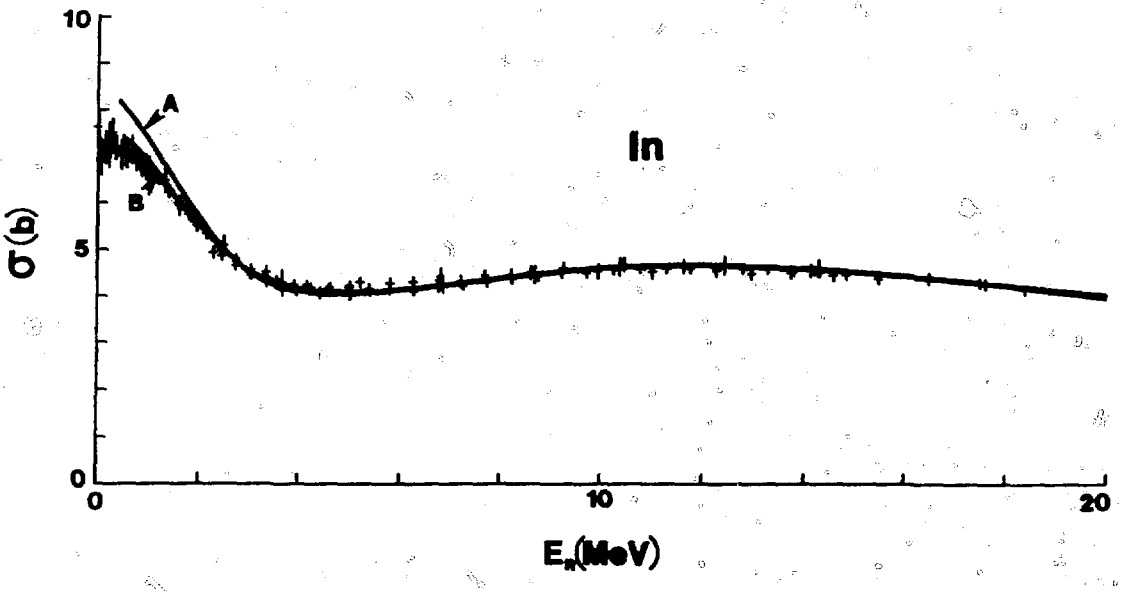


Fig. IV–1. Neutron total cross sections of elemental indium. The data points are energy–averages of various experimental sets, as described in Ref. 3. The light curve indicates the evaluation of Ref. 3. The heavy curves ("A" and "B") show the results of model calculations as described in the text.

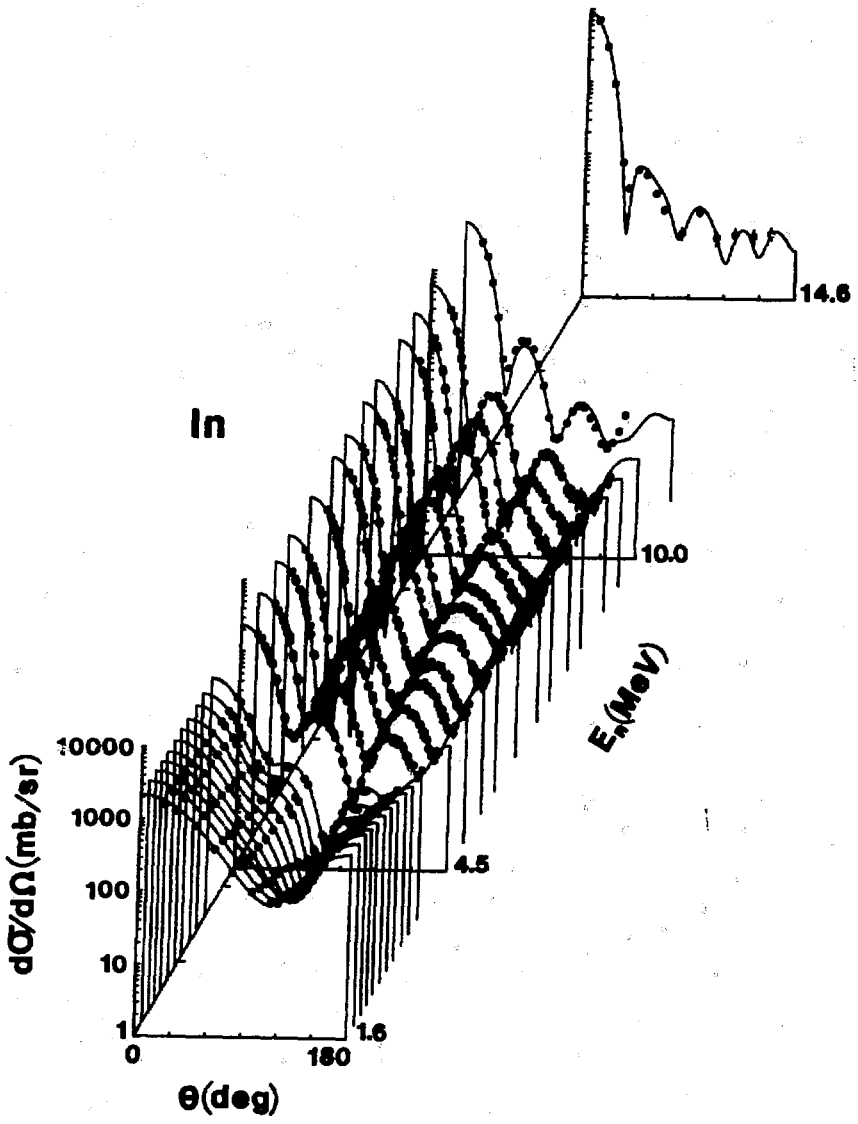


Fig. IV–2. The composite neutron elastic–scattering data base used in the model fitting. The "O" symbols indicate the results of experimental measurements, where energy averages of the 1.5–3.8 MeV data of Ref. 2 are used, together with the present data from 4.5–10 MeV, that of Ref. 19 at 11.1 MeV, and of Ref. 22 at 14.6 MeV. Curves indicate the results of model calculations, as described in the text. The data are given in the laboratory coordinate system.

Fig. IV–2. The procedures started with six–parameter chi–square fits in which the real and imaginary strengths, radii, and diffusenesses were varied. The levels[24] of $^{115}$In up to a 1.5 MeV excitation energy were explicitly taken into account in the calculations using the Hauser–Feshbach[25] approach, corrected for resonance width fluctuations and correlations in the manner described by Moldauer.[26] Higher–energy excitations were incorporated into the calculations using the statistical formalism and parameters of Gilbert and Cameron.[27] It was further assumed that above 5 MeV the observed elastic scattering was entirely shape–elastic, with no compound–elastic contributions. This is a reasonable assumption in view of the very large level density at these higher energies.

The most stable parameter resulting from the six–parameter fitting was the real radius, $r_v$, which decreased slightly with increasing energy. Over the 1.5–14.6 MeV energy range

$$r_v = (1.258 - 0.003 \cdot E) \text{ fm} , \qquad \text{(IV–2)}$$

where, throughout this discussion, the energy, E, is in MeV. The slope is very small and its relative uncertainty fairly large, so that the *E–variation is probably not significant.* However, in the subsequent discussion $r_v$, as given by Eq. IV–2, is used.

The fitting procedure was repeated using a five–parameter chi–square search, varying real and imaginary strengths and diffusenesses, and the imaginary radius. Of the resulting five parameters, the real diffuseness, $a_v$, appeared the most stable and showed no significant energy dependence. Therefore, the $a_v$ results of the fitting procedure were averaged to obtain the value

$$a_v = 0.6404 \text{ fm} . \qquad \text{(IV–3)}$$

This value was accepted for the subsequent SOM fitting procedures.

Using the parameters of Eqs. IV–1 to IV–3, four–parameter fits were carried out. Although the imaginary diffuseness, $a_w$, may increase somewhat with energy, the slope was small, and $a_w$ was taken to be constant with energy, having the value

$$a_w = 0.5798 \text{ fm} . \qquad \text{(IV–4)}$$

This value was then used in three–parameter fitting from which the imaginary radius, $r_w$, was selected to be

$$r_w = (1.305 - 0.003 \cdot E) \text{ fm} , \qquad \text{(IV–5)}$$

where the small energy dependence was chosen equal to that of $r_v$.

Finally, two parameter fitting, with the other parameters taken from Eqs. IV–1 through IV–5, resulted in the real and imaginary potential strengths

$$J_v = (433.4 - 3.7 \cdot E) \text{ MeV fm}^3 \qquad \text{(IV–6)}$$

and

$$J_w = (41.8 + 2.9 \cdot E) \text{ MeV fm}^3 , \qquad \text{(IV–7)}$$

where $J_v$ and $J_w$ are the volume–integrals–per–nucleon of the real and imaginary potentials, respectively. The energy dependence of the individual $J_v$ and $J_w$ values is shown in Figs. IV–3 and IV–4, respectively. Uncertainties associated with $J_v$ and $J_w$ are hard to determine, since they are related by complex error propagation to the difficult-to-determine errors in the underlying data base, particularly in dealing with results other than the present measurements. The uncertainties shown in Figs. IV–3 and IV–4, 1% for $J_v$ and 5% for $J_w$, seem consistent with the scatter of the individual values.

Equations IV–1 to IV–7 define an SOM for the interaction of fast neutrons with indium. The model provides a very good description of the total cross section from 1.5 to 20 MeV, as illustrated in Fig. IV–1. The calculated total cross sections are consistent with the experimentally based evaluation of Ref. 3 to within two percent; i.e., to within approximately the uncertainty in the evaluation alone. This SOM also gives a reasonably good description of the present differential elastic–scattering results, as illustrated in Fig. III–1 and Fig. IV–2. The only major differences are in the depth of the first minimum of the distributions in the energy range $\approx 6 - 8$ MeV. The calculated minimum is very deep and narrow, changing by more than an order of magnitude over an angular range of 3°–4°. Such a "spike–like" behavior is difficult to observe without a specialized experiment. In the present measurements, relatively small scattering samples were used in good geometry, and yet the half–angle subtended by the sample relative to the source was $\approx$ 2.9°. The multiple–event corrections were carried out with a fine 3° Monte-Carlo-calculation mesh, and corrections were made for the remaining angular–resolution effects. Even so, it would be very difficult to detect a cross–section "spike" with the narrow angular character predicted by this SOM. To some extent, the inclusion of the small inelastic scattering to the 336.3 keV state will tend to blunt the minimum, even though the cross section is small and not expected to be sharply forward peaked. However, the experiments do not preclude the existence of such a narrow minimum. This SOM describes the lower–energy, 1.5–3.8 MeV, measured elastic scattering of Ref. 2 very well, as illustrated in Fig. IV–2. Furthermore, it reproduces the rather featureless 0.3–1.5 MeV elastic–scattering distributions previously reported from this laboratory.[1]

Turning to the higher–energy data, the present SOM reproduces the 11.1 MeV results of Ref. 19, except at large scattering angles. On the other hand, the rather rapid rise in this 11.1 MeV cross section at back scattering angles, shown in Fig. IV–2, seems to be inconsistent with what one would expect from an extrapolation of the 10 MeV data. Finally, although this SOM contains no volume absorption, it quite reasonably describes the 14.6 MeV data of Ref. 22, as can be seen in Fig. IV–2. No improvement in the description of the higher–energy data was obtained by the introduction of a volume absorption term in the SOM potential.

Below 1.5 MeV the SOM defined by Eqs. IV–1 to IV–7 tends to predict neutron total cross sections that are increasingly larger than those observed experimentally as the energy decreases, amounting to approximately a 10% overestimate at a few hundred keV. This trend is illustrated by curve "A" in Fig. IV–1. Some of this difference may be experimental, as the measured values were generally not corrected for self–shielding effects and thus may be several percent too small. Also, the predicted s– and p–wave strength functions are both approximately a factor of two larger than those deduced from resonance

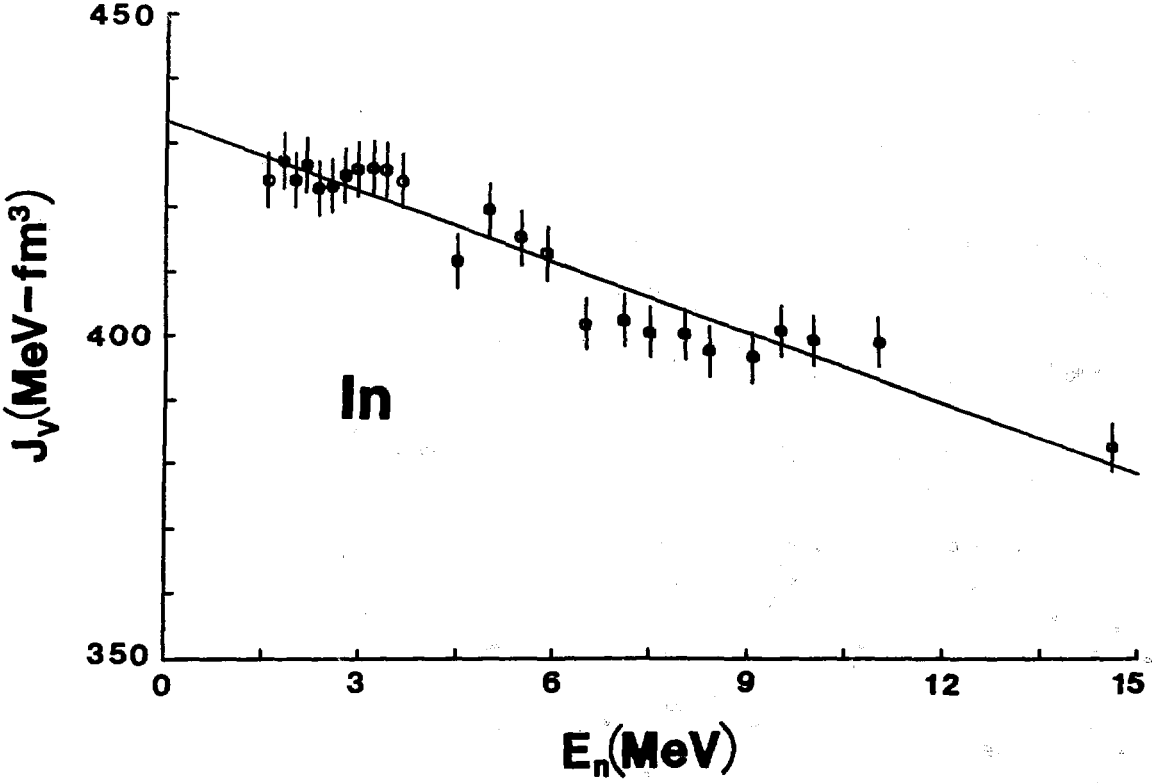


Fig. IV–3. The volume–integral–per–nucleon , $J_v$, of the real potential resulting from the fitting described in the text. Data symbols indicate the results of individual fits to the elastic–scattering data, while the curve indicates the linear least–squares fit given by Eq. IV–6.

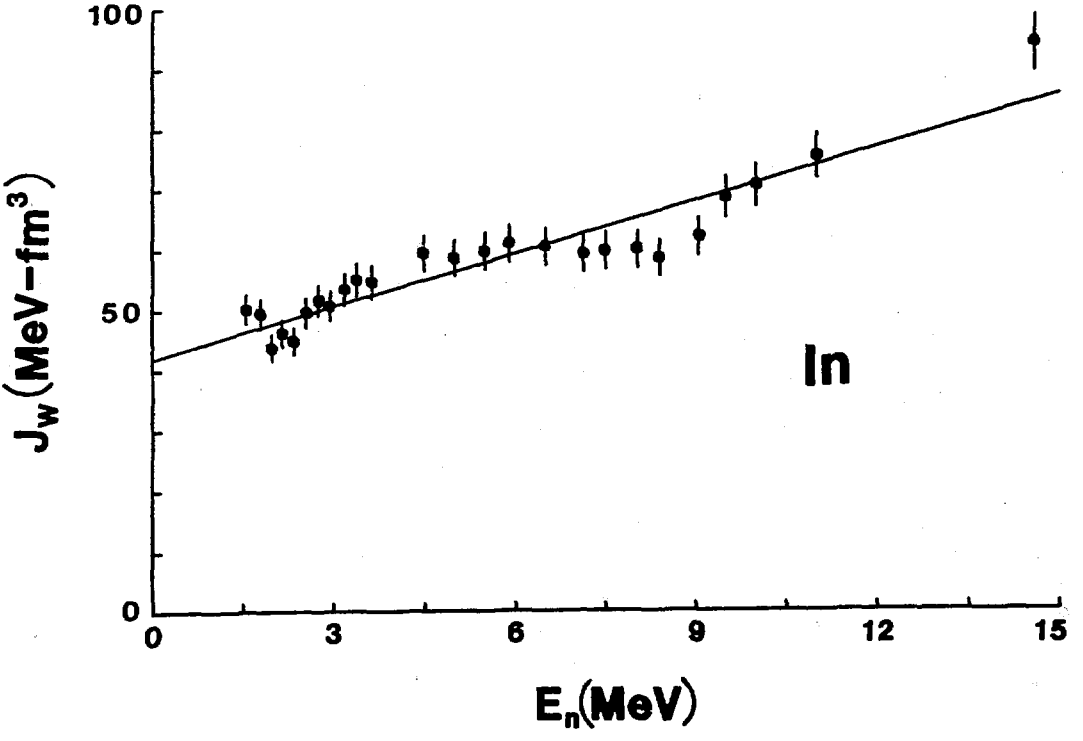


Fig. IV–4. The volume–integral–per–nucleon, $J_w$, of the imaginary potential resulting from the fitting described in the text. The notation is identical to that of Fig. IV–3, except that the curve indicates the result obtained with Eq. IV–7.

measurements.[21] However, it is commonly observed that the imaginary diffuseness, $a_w$, decreases to quite small values as the energy approaches zero,[5-8] rather than remaining energy independent as given by Eq. IV–4. The available experimental information does not permit a clear definition of this behavior in the case of indium. If one approximates the behavior by assuming that $a_w$ decreases in a linear manner from the value of Eq. IV–4 at 2.0 MeV to 0.25 fm at zero energy, and $J_w$ takes the values of Eq. IV–7, a reasonably good description of the observed neutron total cross sections at low energies is obtained, as illustrated by curve "B" in Fig. IV–1. In addition, s– and p–wave strength functions, in units of $10^{-4}$, are now predicted to be 0.34 and 6.41, respectively, compared to the experimentally deduced values[21] of 0.26±0.03 and 3.2±0.6. Thus, deceasing $a_w$ brings the s–wave strength function into good agreement with the experiment, but the calculated value of the more difficult to measure p–wave strength function is still a factor of two larger than deduced from resonance measurements. Finally, the potential scattering length, R′, is predicted to be 6.03 fm, in quite reasonable agreement with the experimental value[21] of (6.55±0.16) fm. Therefore, making $a_w$ decrease, as one lowers the energy, substantially improves the agreement between the low energy calculation and experiment. Moreover, this brings the SOM parameters into better agreement with those deduced from the lower energy,[2] 1.5–3.8 MeV, data alone.

## V. BOUND–STATE PROPERTIES

There is a well–known dispersion relationship linking the real and imaginary OM potentials.[9] In this discussion, we shall use the fact that

$$J_v(E) = J_{HF}(E) + \frac{P}{\pi}\int_{-\infty}^{+\infty} \frac{J_w(E')}{E - E'} \cdot dE', \qquad (V\text{–}1)$$

where $J_v(E)$ and $J_w(E)$ are the volume–integrals–per–nucleon of the total real and imaginary OM interactions, $J_{HF}(E)$ is the Hartree–Fock component of the real potential, and P denotes the principal value of the integral. Mahaux and Sartor[28,29] have exploited this relationship, together with similar expressions relating other radial moments of these interactions, to investigate the shell–model potential. The extrapolation to the bound-state regime gives an additional check on the consistency of the neutron OM potential, since it provides predictions concerning the binding energies of the shell–model states which were not considered in determining the scattering potential. The procedure is geared to finding the properties of single–particle states outside a closed shell, or single hole states in a core. If the shell is not closed, the Pauli exclusion principle will "get in the way" of the prediction of, say, the single–particle energy, $\epsilon_j$, of a j–particle moving outside a partially filled $j^n$ core. On the other hand, if the shell is only slightly occupied in the core, one might still hope to use the extrapolated potential to predict the single–particle energy, since the effect of the exclusion principle would be small. Because the pairing force favors occupation of the high j–orbitals,[30] one might hope that near the middle of the $N = 50 - 82$ shell, consisting of $d_{5/2}$, $g_{7/2}$, $h_{11/2}$, $s_{1/2}$, and $d_{3/2}$ neutron orbitals, the low–spin states, $s_{1/2}$ and $d_{3/2}$, would have little population, and that their binding energies might be reasonably predicted by this extrapolation. In this section, we shall examine to what extent this is true for neutrons moving outside the $N = 66$ ($^{115}$In) and $N = 64$ ($^{114}$Sn) cores.

In order to use Eq. V–1, $J_w$ must be known for all energies. In the following calculations, it is assumed that:

(i) $J_w$ is continuous and symmetric about the Fermi energy, $E_F$.

(ii) For $2 \cdot E_F \leq E \leq 0$, $J_w$ is proportional to $(E - E_F)^2$.

(iii) For $0 \leq E \leq E_m$, $J_w$ is given by Eq. IV–7. $E_m$ is the energy at which the expression for $J_w$ is equal to that obtained using Rapaport's[31] global parameters (for $^{115}$In, $E_m = 14.42$ MeV).

(iv) For $E_m \leq E \leq 30$ MeV, $J_w$ has the linear energy dependence and values obtained using Rapaport's model.[31]

(v) For $E \geq 30$ MeV, $J_w$ is taken to be constant at its 30 MeV value.

With these assumptions, the contribution of the principal–value integral in Eq. V–1 was evaluated and a best fit to the experimental values of $J_v(E)$, shown in Fig. IV–3, was made, assuming that

$$J_{HF} = J_1 + J_2 \cdot E, \qquad \text{(V–2)}$$

where $J_1$ and $J_2$ are constants.

The resulting expression for $J_v$ was assumed to hold true for both positive and negative energies and, consequently, can be used to predict the real shell–model potential strength. In carrying out the OM fitting described in Section IV, it was found that the diffuseness of the real well, Eq. IV–3, was energy independent. Furthermore, although a small energy dependence was assumed for $r_v$, Eq. IV–2, it is probably not significant, as noted above. Therefore, in discussing bound states it is assumed that the shell–model potential has a constant diffuseness given by Eq. IV–3, and a constant radius $r_v = 1.258$ fm, the $E = 0$ value of Eq. IV–2. The shell–model spin–orbit potential is taken to be the Thomas form, described by the parameters of Eq. IV–1.

The single–particle energies for a neutron moving outside the $^{115}$In core are difficult to determine, since the system is the odd–odd nucleus $^{116}$In. The first and second excited states[32] of $^{116}$In, which have $I^\pi$ values of $5^+$ and $4^+$, show up strongly in stripping with an $\ell = 0$ pattern, and probably are the two possible spin states of a valence $s_{1/2}$ neutron coupling to the $9/2^+$ ground state of the $^{115}$In core. Using the average energy of these two states, in conjunction with the binding–energy tables,[33] one concludes that the $s_{1/2}$ neutron is bound to the the core by about 6.6 MeV. The next expected single–particle level would be the $d_{3/2}$, which can couple to $^{115}$In to give spins ranging from $3^+$ to $6^+$. States with $J^\pi$ values of $3^+$, $4^+$, $5^+$, and $6^+$ are seen in $^{116}$In at excitation energies of 508, 426, 313, and 649 keV, respectively. All except the $4^+$ state show strong $\ell = 2$ stripping patterns. Unfortunately, none of the $4^+$ states observed in the (d,p) reaction[32] show an $\ell = 2$

character, so that clear evidence for all states of the $(g_{9/2}^{-1}, d_{3/2}^{1})$ quartet cannot be found. On the other hand, a shell–model calculation using the Schiffer–True interaction[34] indicates that the $4^+$ member of the quartet should lie about 120 keV above the $5^+$ level, in good agreement with the observed 426 keV $4^+$ state. Thus, using either the average of the four experimental energies quoted above, or using only the $3^+$, $5^+$, and $6^+$ states, which exhibit $\ell = 2$ stripping patterns, one concludes that the $d_{3/2}$ single–particle orbit is bound by about 6.3 MeV to the $^{115}$In core.

Since the $d_{5/2}$ and $g_{7/2}$ neutron states are the first to fill in the N = 50–82 region[35] and hold 14 particles, one might expect that the $h_{11/2}$ neutron state ($\nu h_{11/2}$) is not strongly populated in the core, and hence the extrapolation procedure might provide a reasonable estimate of its energy. The proton hole ground state ($\pi g_{9/2}^{-1}$) of $^{115}$In can couple with the $\nu h_{11/2}$ level to give spins ranging from $1^-$ to $10^-$. Candidates for all these levels, except the $1^-$, $2^-$ and $10^-$ states, are seen in $^{116}$In below 750 keV.[32] The average of these observed energies implies that the $h_{11/2}$ orbit is bound to the $^{115}$In core by about 6.3 MeV. On the other hand, if one uses the Schiffer–True interaction[34] to predict the position of the other $(\pi g_{9/2}^{-1}, \nu h_{11/2})$ states, and combines them with the observed $3^-$ to $9^-$ levels, one finds that the binding energy to the core is about 5.9 MeV.

Assuming that the $g_{7/2}$ and $d_{5/2}$ orbits are full, one can learn about the binding of the hole states from $^{114}$In. The ground–state spin of this nucleus[36] is $1^+$, and is interpreted to arise from the $(\pi g_{9/2}^{-1}, \nu g_{7/2}^{-1})$ configuration. According to the Schiffer–True interaction,[34] this state lies about 1 MeV lower than the $2^+$ member of the octet of states arising from this configuration, and more than 2 MeV lower than the other possible octet members, $I^\pi = 3^+$ to $8^+$. If one uses the experimental energy of the $1^+$ state alone, one concludes that the $g_{7/2}$ hole is bound by about 9 MeV to the $^{115}$In core, whereas if one combines the $1^+$ binding energy with the predicted Schiffer–True energies for the rest of the states in the multiplet, one obtains about 10.3 MeV for this binding. Finally, there is little evidence for the $(\pi g_{9/2}^{-1}, \nu d_{5/2}^{-1})$ sextet. The Schiffer–True interaction predicts that the lowest state would be $7^+$, and there is some evidence for a $7^+$ level at 642 keV in $^{114}$In. If this is taken for the $d_{5/2}^{-1}$ energy, one concludes that the $d_{5/2}$ hole is bound by about 9.7 MeV. If the Schiffer–True potential is used to calculate the energies of all other spins of this configuration, and they are normalized to the yrast $7^+$ level, one concludes that the $d_{5/2}$ hole–state binding energy is about 10.1 MeV.

The binding energies deduced from the experimental results and from the data, together with the Schiffer–True interaction, are shown in Table V–1. The well depths needed to give these binding energies are also shown in the table and are compared with the values predicted by Eq. V–1. In making these predictions, the Fermi energy, $E_F$, was taken to be

$$E_F = \frac{1}{2}\cdot(\epsilon_s + \epsilon_g)\,. \qquad \text{(V–3)}$$

Table V–1

Binding energies (BE) of the $s_{1/2}$, $d_{3/2}$ and $h_{11/2}$ particle states, and the $g_{7/2}$ and $d_{5/2}$ hole states relative to the $^{115}$In and $^{114}$Sn cores are tabulated. As discussed in the text, the position of the $d_{5/2}$ hole state in $^{114}$In is very tenuous. In columns headed "Experiment", only the observed states are considered. In the fourth column, the Woods–Saxon well depths needed to reproduce the BE's are shown when the diffuseness and radius are 0.6404 fm and 1.258 fm, respectively, and the spin–orbit potential is of the Thomas form with the parameters of Eq. IV–1. In the fifth column, the well depths predicted from the neutron-scattering analysis using Eq. V–1 are given. Under the heading "Schiffer–True", the experimental data are augmented, as discussed in the text, to include the shell–model predictions for states of the various multiplets that have not been experimentally seen. For binding to the $^{114}$Sn core, only experimental data are used. All energies are in MeV.

| Core | State | BE | Experiment Well Depths Required | Predicted |
|---|---|---|---|---|
| $^{115}$In | $s_{1/2}$ | 6.6 | 45.1 | 45.5 |
| | $d_{3/2}$ | 6.3 | 44.7 | 45.6 |
| | $h_{11/2}$ | 6.3 | 47.3 | 45.6 |
| | $g_{7/2}$ | 9.0 | 47.0 | 44.0 |
| | $d_{5/2}$? | 9.7 | 47.3 | 43.6 |
| | State | BE | Schiffer–True Well Depths Required | Predicted |
| | $s_{1/2}$ | 6.6 | 45.1 | 45.8 |
| | $d_{3/2}$ | 6.3 | 44.7 | 46.0 |
| | $h_{11/2}$ | 5.9 | 46.8 | 46.2 |
| | $g_{7/2}$ | 10.3 | 48.7 | 43.8 |
| | $d_{5/2}$? | 10.1 | 47.9 | 43.9 |
| | State | BE | Experiment Well Depths Required | Predicted |
| $^{114}$Sn | $s_{1/2}$ | 7.3 | 46.4 | 46.3 |
| | $d_{3/2}$ | 6.9 | 45.8 | 46.5 |
| | $h_{11/2}$ | 6.8 | 48.2 | 46.6 |
| | $g_{7/2}$ | 10.4 | 49.0 | 44.8 |
| | $d_{5/2}$ | 10.7 | 48.9 | 44.7 |

For the $s_{1/2}$, $d_{3/2}$, and $h_{11/2}$ particle states, the agreement between required and predicted well depths is reasonably good, the rms error being 1.1 MeV when the experimental results alone are used, and 0.9 MeV when the data is augmented with the Schiffer–True predictions. This is similar to the rms deviation in $^{51}$V, which was about 1.1 MeV when all the particle and hole states were included. On the other hand, the required depths for the hole states are at least 3 MeV deeper than those predicted by Eq. V–1.

To see whether or not the hole–state potential difference arises merely from the odd–odd nature of $^{116}$In, the required well depths needed to explain the data in the neighboring odd–A tin isotopes were examined. Binding energies relative to the even–even $^{114}$Sn nucleus can be obtained from a knowledge of the states in $^{113}$Sn and $^{115}$Sn. In this case, the fourteen valence neutrons in the $^{114}$Sn core are assumed to occupy the $(\nu\, d_{5/2})^6(\nu\, g_{7/2})^8$ configuration outside the closed N = Z = 50 shell. The energies and spectroscopic factors given in the Nuclear Data Sheets[24] for $^{115}$Sn allow one to obtain the single–particle energies defined by

$$\epsilon_j = \sum_i S_{ji} \cdot E_{ji} \Big/ \sum_i S_{ji} \ , \qquad \text{(V–4)}$$

where $S_{ji}$ is the spectroscopic factor for populating the $i^{th}$ state with spin j and energy $E_{ji}$. Combining these results with the binding–energy tables[23] leads to the $s_{1/2}$, $d_{3/2}$, and $h_{11/2}$ particle–state energies, relative to $^{114}$Sn, shown in Table V–1. In the same manner, the $g_{7/2}$ and $d_{5/2}$ energies are obtained from the data[27] on $^{113}$Sn.

In order to use the $^{116}$In scattering results to make predictions for well depths needed in $^{114}$Sn, the following changes were made:

(i) According to Rapaport's global model,[31] the isovector contribution should change $J_v$ in going from $^{116}$In to $^{114}$Sn by

$$\Delta J_v = (5.25 - 0.044 \cdot E) \text{ MeV fm}^3 \ . \qquad \text{(V–5)}$$

This contribution should be added to the $J_v$ values shown in Fig. IV–3 so as to make them appropriate for $^{114}$Sn.

(ii) Again using the global model,[31] one finds that $\Delta J_w = 0.26$ MeV–fm$^3$. Thus, for $^{114}$Sn

$$J_w = (42.06 + 2.9 \cdot E) \text{ MeV–fm}^3 \ . \qquad \text{(V–6)}$$

Once these changes are made, the procedure is exactly as already discussed.

The results for the $^{114}$Sn core are given in Table V–1. In the fourth column, the Woods–Saxon well depths required to give the observed binding energies are quoted. In the fifth column, the predicted well depths, found by use of Eq. V–1 when the Fermi energy is given by Eq. V–3, are listed. For particle states, the agreement between required and predicted well depths is quite reasonable, with the rms deviation between the two

being about 1 MeV. However, once more, the well depths necessary to reproduce the hole–state energies are almost 10% greater than the values predicted by the use of Eq. V–1.

Near the middle of the 50–82 neutron shell, one concludes that, when the OM potential found by fitting the indium data is extrapolated to the bound–state regime, quite reasonable predictions can be made for the shell–model potential needed to give the experimental energies of the $h_{11/2}$, $d_{3/2}$, and $s_{1/2}$ particle states. On the other hand, the extrapolated potential cannot be used to predict the energies of the $d_{5/2}$ and $g_{7/2}$ hole states. This indicates that the particle states have orbits with sufficiently small occupation probability that the exclusion principle does not get in the way, whereas the $d_{5/2}^{-1}$ and $g_{7/2}^{-1}$ levels are not "true" hole states, and have an occupational probability sufficiently different from unity that the exclusion principle becomes a factor.

## VI. DISCUSSION

Listed in Table VI–1 are the values of $J_v$ and the radii, $r_v$, of the SOM potential appropriate for the scattering of 8 MeV neutrons from various nuclei, including the indium results presented in this paper. From an inspection of the Table, it is clear that $r_v$ decreases as the mass, A, increases—a result similar to that found by Moldauer[38] when he attempted to fit very low energy neutron data. A least–squares fit was made to these radii assuming that

$$r_v = r_0 + r_1/A^{1/3} \text{ fm} , \qquad \text{(VI–1)}$$

in other words, assuming the nuclear radius, $R_v$, is proportional to $A^{1/3}$ plus a constant. When

$$r_0 = 1.1476 \text{ fm} \quad \text{and} \quad r_1 = 0.4416 \text{ fm} \qquad \text{(VI–2)}$$

the values listed under "Systematics" in Table VI–1 are obtained. The fit to the empirically determined SOM radii is excellent, with an rms deviation between theory and experiment of approximately 0.5%. Furthermore, the values of $r_0$ and $r_1$ are similar to those given by Moldauer,[38] who obtained 1.16 fm and 0.6 fm, respectively, for these quantities.

In a similar way, $J_v$ decreases as A increases. If one attempts to fit the empirical values with the relationship

$$J_v = J_0 \cdot [1 - \xi(N–Z)/A] , \qquad \text{(VI–3)}$$

one finds $J_0 = 486.8$ MeV–fm$^3$ and $\xi = 1.04$. These values are similar to those found by Holmqvist and Wiedling,[39] who also studied the scattering of 8 MeV neutrons from a number of nuclei and found $J_0 = 480$ MeV–fm$^3$ and $\xi = 0.98$. They are also quite close to the 11.1 MeV results of Ferrer et al.,[19] who obtained $J_0 = (495 \pm 30)$ MeV–fm$^3$ and $\xi = 0.95$. On the other hand, the nucleon–nucleon scattering data indicates that $\xi$ should

Table VI–1

Values of $r_v$, $J_v$, $r_w$, and $J_w$ obtained by fitting the data for the elastic–scattering of 8 MeV neutrons from the nuclei listed in the first column. A spherical OM was assumed. The last two "Systematics" columns give the values of $r_v$ and $J_v$ predicted with Eqs. VI–1, VI–2, and VI–4 of the text.

| Nucl. Ref. | Specific SOM | | | | Systematics | |
|---|---|---|---|---|---|---|
| | $r_v$[a] | $J_v$[b] | $r_w$[a] | $J_w$[b] | $r_v$[a] | $J_v$[b] |
| $^{51}$V/8 | 1.2680 | 440.4 | 1.2997 | 68.9 | 1.2667 | 451.3 |
| $^{58}$Ni/46 | 1.2538 | 462.9 | 1.2000 | 104.8 | 1.2617 | 461.7 |
| $^{59}$Co/7 | 1.2624 | 454.8 | 1.2119 | 85.6 | 1.2610 | 448.6 |
| $^{89}$Y/5 | 1.2400 | 424.5 | 1.3296 | 66.5 | 1.2465 | 423.9 |
| $^{90}$Zr/47 | 1.2593 | 431.9 | 1.3388 | 66.3 | 1.2461 | 426.6 |
| $^{93}$Nb/4 | 1.2500 | 426.3 | 1.3000 | 75.9 | 1.2451 | 423.7 |
| $^{115}$In | 1.2340 | 400.1 | 1.2810 | 65.0 | 1.2384 | 410.1 |
| $^{209}$Bi/6 | 1.2200 | 385.5 | 1.3102 | 43.0 | 1.2220 | 380.9 |

[a] Radii are given in fm.
[b] Volume–integrals–per–nucleon, $J_i$, are given in MeV–fm$^3$.

be[40] about 0.48, and the (p,n) results are consistent[41] with a value of $\xi = 0.4$, both about a factor of two smaller than obtained from the analysis of the 8 and 11 MeV neutron-scattering data. However, the neutron–scattering results can be brought into reasonable agreement with the (p,n) and two–body data if one takes into account the radius variation proposed in Eq. VI–1. If one sets

$$J_v = K_o \cdot [1 - \xi(N-Z)/A] \cdot (r_o + r_1/A^{1/3})^3 \ , \qquad \text{(VI–4)}$$

with $r_o$ and $r_1$ having the values given in Eq. VI–2, one finds $K_o = 234.2$ MeV–fm$^3$ and $\xi = 0.53$. The fit obtained in this way, and given in Table VI–1, leads to an rms deviation between calculated and observed values of $J_v$ of 6.3 MeV–fm$^3$, the same as obtained when the conventional fit, Eq. VI–3, is made.

Thus, the real SOM potential obtained from the indium data fits in quite nicely with the values obtained from the study of other nuclei throughout the periodic table. Furthermore, the indium value of $a_v = 0.6404$ fm is similar to the average $a_v$ value, 0.67 fm, for the other nuclei listed in Table VI–1.

In Table VI–1, $r_w$ and $J_w$, the radius and volume–integral–per–nucleon of the imaginary SOM potential at 8 MeV, are also given. There is no evidence for a smooth variation of these quantities with mass number A, and this is consistent with the fact that the imaginary portion of the SOM is expected to be sensitive to nuclear structure. The values of $J_w$ can, however, be divided into three groups: (i) $J_w < 50$, (ii) $50 < J_w < 80$, and (iii) $J_w > 80$ MeV–fm$^3$. The only nucleus in this list in category (i) is $^{209}$Bi. It is a doubly–closed–shell–plus–one nucleus, and the small value of $J_w$ is consistent with the fact that the $^{208}$Pb core is a very stable structure. Indium falls in the second group, which includes $^{51}$V, $^{89}$Y, $^{90}$Zr, and $^{93}$Nb. The first three members of this group can be adequately described by the spherical shell model,[42,43] and this implies that the low–lying states in $^{93}$Nb and $^{115}$In should also be understandable in terms of this model. For nuclei in this group, the cores are more easily excited than those near the doubly–closed $Z = 82$, $N = 126$ shell and, consequently, $J_w$ is larger. Finally, the two nuclei with $J_w > 80$ MeV–fm$^3$ (namely, $^{58}$Ni and $^{59}$Co) not only have anomalously large values of $J_w$, but they also differ from other imaginary SOM potentials in two significant respects: (i) in the energy range $0 < E$ 10 MeV, $J_w$ decreases as the incident energy increases, and (ii) $r_w < r_v$. These effects seem to imply that one is attempting to describe a deformed nucleus with an SOM.[7,44]

Thus the imaginary SOM potential for indium has a $J_w$ value consistent with other spherical nuclei. Furthermore, the empirical value of $r_w$ for indium is only slightly larger than the average value, 1.3157 fm, obtained for other nuclei in this class. The diffuseness, $a_w$, of the derivative Woods–Saxon interaction varies significantly for the six nuclei considered to be spherical, ranging from 0.3933 fm for $^{89}$Y to 0.5798 fm for indium. The imaginary diffuseness obtained for indium is about 0.12 fm greater than the average for the other spherical nuclei and, undoubtedly, this reflects differences in the nuclear structure.

In extrapolating the OM to the bound–state regime, only the volume–integral–per–nucleon of the imaginary interaction was used, and attention was not given to the detailed form of the potential. For the so–called particle states, $s_{1/2}$, $d_{3/2}$, and $h_{11/2}$, the extrapolated potential gave Woods–Saxon well depths in satisfactory agreement with those needed to reproduce the observed binding energies. As pointed out in Sec. IV, the scattering data fitted in our interpretation were not particularly sensitive to the spin–orbit interaction. However, with the exception of the $s_{1/2}$ level, the binding energies are quite sensitive to this potential. For example, if one merely increases $V_{so}$ from 5.5 to 6.0 MeV, the required well depths needed to reproduce the observed binding of the $d_{3/2}$ and $h_{11/2}$ states to the $^{114}$Sn core become 46.0 and 47.9 MeV, respectively, and this reduces the rms deviation between the required and predicted well depths from 1.0 to 0.8 MeV. Thus, the bound particle states seem to indicate a slightly stronger spin–orbit potential than that deduced from neutron–scattering data.

Turning to the $d_{5/2}$ and $g_{7/2}$ hole states, the extrapolated OM potential does not explain the observed binding energies. This undoubtedly stems from at least two sources: First, the Pauli exclusion principle "gets in the way", and, secondly, the core configuration is changed when the hole–state is produced. To check this, the $^{115}$In OM potential was extrapolated to the $^{132}$Sn nucleus by using Rapaport's[31] global values for the isovector

potential strengths. In addition, since $J_w$ is, in first order, proportional to $A^{-1/3}$, Eq. IV–7 was scaled by the factor $(115/132)^{1/3}$. The energies of the hole states in $^{131}$Sn have been deduced by Fogelberg and Blomqvist.[45] and when these data are combined with the binding-energy tables,[33] one finds that the required well depths for the $d_{3/2}^{-1}$, $h_{11/2}^{-1}$, $s_{1/2}^{-1}$, $d_{5/2}^{-1}$, and $g_{7/2}^{-1}$ states are 42.8, 44.9, 43.3, 43.0 and 44.4 MeV, respectively. These are to be compared with the predicted values, when $E_F = -6.5$ MeV, of 43.5, 43.4, 43.4 42.9, and 42.6 MeV. Thus, the rms deviation between predicted and required well depths is about 1.1 MeV, the same as that found[8] for $^{51}$V. Therefore, when one goes to a truly closed–shell nucleus, where rearrangement of the core is small and the exclusion principle does not get in the way, the shell–model potential obtained by the extrapolation of the $^{115}$In OM deduced from the neutron scattering provides a good description of the bound–state data.

## REFERENCES


1. W. G. Vonach and A. B. Smith, Nucl. Phys. 78 389 (1966).

2. A. B. Smith, P. T. Guenther and J. F. Whalen, Argonne National Laboratory Report, ANL/NDM–78 (1982); see also A. Smith, P. Guenther, J. Whalen, I. Van Heerden and W. McMurray, J. Phys. G11 125 (1985).

3. A. B. Smith, S. Chiba, D. L. Smith, J. W. Meadows, P. T. Guenther, R. D. Lawson and R. J. Howerton, Argonne National Laboratory Report, ANL/NDM–115 (1990).

4. A. B. Smith, P. T. Guenther and R. D. Lawson, Nucl. Phys. A455 344 (1986).

5. R. D. Lawson, P. T. Guenther and A. B. Smith, Phys. Rev. C34 1599 (1986).

6. R. D. Lawson, P. T. Guenther and A. B. Smith, Phys. Rev. C36 1298 (1987).

7. A. B. Smith, P. T. Guenther and R. D. Lawson, Nucl. Phys. A483 50 (1988).

8. R. D. Lawson, P. T. Guenther and A. B. Smith, Nucl. Phys. A493 267 (1989).

9. G. R. Satchler, ***Direct nuclear reactions***, Clarendon Press, Oxford (1983).

10. P. E. Hodgson, ***Nuclear reactions and nuclear structure***, Clarendon Press, Oxford (1971).

11. A. Smith, P. Guenther, R. Larson, C. Nelson P. Walker, and J. Whalen, Nucl. Instr. Methods 50 277 (1967).

12. C. Budtz–Jorgensen, P. Guenther, A. Smith, J. Whalen, W. McMurray, M. Renan, and I. Van Heerden, Z. Phys. A319 47 (1984).

13. P. Guenther, A. Smith and J. Whalen, Phys. Rev. C12 1797 (1976).

14. M. Drosg, IAEA–TECDOC–410, 239, IAEA Press, Vienna (1987).

15. A. Smith, P. Guenther, and R. Sjoblum, Nucl. Instr. Methods 140 397 (1977).

16. H. Condé, A. Smith and A. Lorenz, eds., Nuclear Standards File, IAEA Tech Report 227, IAEA Press, Vienna (1983).

17. A. B. Smith, MONTE–SPHERE and MONTE–POLY, Monte–Carlo correction codes, unpublished memorandum (1988), available from the author.

18. D. L. Smith, Argonne National Laboratory Report, ANL/NDM–26 (1976).

19. J. C. Ferrer, J. D. Carlson and J. Rapaport, Nucl. Phys. A275 325 (1977).

20. B. Holmqvist and T. Wiedling, Aktiebolaget Atomenergi Report, AE–430 (1971).

21. S. F. Mughabghab, M. Divadeenam and N. E. Holden, ***Neutron cross sections***, Vol.–1, Part–A, Academic Press, New York (1981).

22. L. F. Hansen, F. S. Dietrich, B. A. Pohl, C. H. Poppe and C. Wong, Phys. Rev. C31 31 (1985).

23. G. V. Gorlov, N. S. Lebedeva and V. M. Morosov, private communication.

24. J. Blachot and G. Marguier, Nucl. Data Sheets 52 565 (1987).

25. W. Hauser and H. Feshbach, Phys. Rev. 87 366 (1952).

26. P. A. Moldauer, Nucl. Phys. A344 185 (1980).

27. A. Gilbert and A. Cameron, Can. J. Phys. 43 1446 (1965).

28. C. Mahaux and R. Sartor, Phys. Rev. Lett. 57 3015 (1986).

29. C. Mahaux and R. Sartor, Nucl. Phys. A484 205 (1988); see also references cited therein.

30. L. S. Kisslinger and R. A. Sorensen, Rev. Mod. Phys. 35 853 (1963).

31. J. Rapaport, Phys. Reports 87 25 (1982).

32. J. Blachot J. P. Husson, J. Oms, G. Marguier and F. Hass, Nucl. Data Sheets 32 287 (1981).

33. A. H. Wapstra and K. Bos, At. Data and Nucl. Data Tables 19 177 (1977).

34. J. P. Schiffer and W. W. True, Rev. Mod. Phys. 48 191 (1976).

35. E. J. Schneid, A. Prakash and B. L. Cohen, Phys. Rev. 156 1316 (1967).

36. J. Blachot and G. Marguier, Nucl. Data Sheets 35 375 (1982).

37. J. Lyttkens, K. Nilson and L. P. Ekstrom, Nucl. Data Sheets 33 1 (1981).

38. P. A. Moldauer, Nucl. Phys. 47 65 (1963).

39. B. Holmqvist and T. Wiedling, Nucl. Phys. A188 24 (1972).

40. G. W. Greenlees, W. Makofske and G. J. Pyle, Phys. Rev. C1 1145 (1970).

41. C. J. Batty, E. Friedman and G. W. Greenlees, Nucl. Phys. A127 368 (1969).

42. R. D. Lawson, ***Theory of the nuclear shell model***, Clarendon Press, Oxford (1980).

43. S. Cohen, R. D. Lawson, M. H. Macfarlane and M Soga, Phys. Lett. 10 195 (1964).

44. A. B. Smith, P. T. Guenther and J. Whalen, Nucl. Phys. A415 1 (1984).

45. B. Fogelberg and J. Blomqvist, Phys. Lett. 137B 20 (1984).

46. A. B. Smith, P. T. Guenther and R. D. Lawson, to be published.

47. S. Chiba, P. T. Guenther, R. D. Lawson and A. B. Smith, to be published.

48. C. H. Johnson, D. J. Horen and C. Mahaux, Phys. Rev. C36 2252 (1987).

## APPENDIX

Because the $^{114}$Sn nucleus does not have a particularly good $(d_{5/2})^6(g_{7/2})^8$ closed–shell structure, the basic assumptions underlying the use of the OM potential to extract the occupation probabilities for bound states is not entirely correct. However, it is of interest to examine how well these probabilities can be predicted on the basis of the closed–shell approximation, and this calculation is presented here.

In the preceding discussion only the volume integral of the imaginary potential was used in extrapolating to the shell–model regime. However, the prediction of occupation probabilities for the shell–model orbits requires a more detailed knowledge of the potential. For the hole states, the occupation probability is given by[48]

$$N_j = \int_0^\infty u_j^2\, r^2\, dr \left[ 1 - \left[ \frac{d}{dE} \left( \frac{P}{\pi} \int_{E_F}^{\infty} \frac{W(r,E')}{E - E'}\, dE' \right) \right]_{E=\epsilon_j} \right], \qquad \text{(A–1)}$$

and for the particle states by

$$N_j = \int_0^\infty u_j^2\, r^2\, dr \left[ \frac{d}{dE} \left( \frac{P}{\pi} \int_{-\infty}^{E_F} \frac{W(r,E')}{E - E'}\, dE' \right) \right]_{E=\epsilon_j}. \qquad \text{(A–2)}$$

In these equations, $E_F$ is the Fermi energy given by Eq. V–3, $u_j$ is the bound–state radial wave function for a neutron in the orbit j, normalized so that $\int_0^\infty u_j^2\, r^2\, dr = 1$, and $\left[ \ldots \right]_{E=\epsilon_j}$ indicates that the bracketed quantity is to be evaluated at $\epsilon_j$, the binding energy of the particle in orbit j.

To deduce the values of $N_j$ for $^{114}$Sn, one makes the same assumptions about $W(r,E')$ as were previously made about $J_w(E)$. However, in addition one assumes that $W(r,E')$ is made up of a volume plus surface absorption. The volume absorption was taken from Rapaport's global model[31] and, for simplicity, was assumed to increase linearly with energy [$W_0 = (-4.3 + 0.38 \cdot E)$ MeV] between 11.3 and 30 MeV. Above 30 MeV, a constant strength of 7.1 MeV was taken. For the surface potential, a constant diffuseness, given by Eq. IV–4, and a value of $r_w = 1.3$ fm were assumed for all energies. The potential strength was then determined so that Eq. V–6 was satisfied. Above 11.3 MeV, the surface potential strength was adjusted so that the sum of surface and volume imaginary potentials had the volume–integral–per–nucleon equal to the value given by Eq. V–6. The surface imaginary strength obtained in this way is equal to Rapaport's global strength at 15 MeV. For energies greater than this, the global energy dependence was assumed.

In Table A–1, the contributions to $N_j$ from volume and surface absorption are given separately. The $s_{1/2}$, $d_{3/2}$, and $h_{11/2}$ are particle states, and the $g_{7/2}$ and $d_{5/2}$ are hole states. The experimental values given in the table are those of Schneid et al.[35] and were obtained from a combination of (d,p) and (d,t) data (see Table X of their paper). Theory

and experiment are in good agreement for the $h_{11/2}$ and $g_{7/2}$ orbitals, but the predicted $s_{1/2}$ strength is only about half the observed value. However, the extraction of $N_j$ from stripping and pickup data depends sensitively on the tail of the nuclear wave function. Since the $s_{1/2}$ orbit peaks at the center of the nucleus, where the concept of independent particle motion is least likely to be valid, the "tail normalization" may be incorrect and, hence, substantially affect the extraction of the $s_{1/2}$ occupation probability. Finally, for $\ell = 2$ states, the predicted value of $N_j$ is larger than experiment for the $d_{5/2}$ level and smaller than the data for the $d_{3/2}$ state. Since it is difficult to distinguish between $d_{3/2}$ and $d_{5/2}$ levels, perhaps a more meaningful comparison is the total number of particles in the $^{114}$Sn core with $\ell = 2$. The experimental results indicate there are about 4.8 particles, whereas the theory gives 5.7. In view of the approximately 30% uncertainty in extracting these numbers from the data, theory and experiment are in reasonable agreement for the total number of $\ell = 2$ nucleons.

Table A–1

Comparison of experimental and theoretical occupation probabilities for various states in $^{114}$Sn. The theoretical estimates are based upon Eqs. A–1 and A–2, and the volume and surface imaginary–potential contributions to these integrals are listed separately. The experimental results are from Ref. 35.

| | State | $s_{1/2}$ | $d_{3/2}$ | $h_{11/2}$ | $g_{7/2}$ | $d_{5/2}$ |
|---|---|---|---|---|---|---|
| | Volume Imag. | 0.051 | 0.053 | 0.058 | 0.061 | 0.056 |
| | Surface Imag. | 0.074 | 0.073 | 0.079 | 0.076 | 0.071 |
| $N_j$ | Theory | 0.125 | 0.126 | 0.137 | 0.863 | 0.873 |
| | Exp. | 0.26 | 0.31 | 0.17 | 0.86 | 0.60 |